Persistent earthquake clusters and gaps from slip on irregular faults

TOM PARSONS
US Geological Survey, MS-999, 345 Middlefield Rd., Menlo Park, California 94025, USA
e-mail: tparsons@usgs.gov

Published online: 9 December 2007; doi:10.1038/ngeo.2007.36

Earthquake-producing fault systems like the San Andreas fault in California show self-similar structural variation[1]; earthquakes cluster in space, leaving aseismic gaps between clusters. Whether gaps represent overdue earthquakes or signify diminished risk is a question with which seismic-hazard forecasters wrestle[1–5]. Here I use spectral analysis of the spatial distribution of seismicity along the San Andreas fault (for earthquakes that are at least 2 in magnitude), which reveals that it obeys a power-law relationship, indicative of self-similarity in clusters across a range of spatial scales. To determine whether the observed clustering of earthquakes is the result of a heterogeneous stress distribution, I use a finite-element method to simulate the motion of two rigid blocks past each other along a model fault surface that shows three-dimensional complexity on the basis of mapped traces of the San Andreas fault. The results indicate that long-term slip on the model fault generates a temporally stable, spatially variable distribution of stress that shows the same power-law relationship as the earthquake distribution. At the highest rates of San Andreas fault slip (40 mm yr^{-1}), stress patterns produced are stable over a minimum of 25,000 years before the model fault system evolves into a new configuration. These results suggest that although gaps are not immune to rupture propagation they are less likely to be nucleation sites for earthquakes.

At first glance, California's spatial earthquake distribution seems random, with clusters of activity interspersed by broad gaps (Fig. 1). However, earthquake maps tend to have underlying self-similar organization, having the same spatial appearance regardless of scale[1]. Earthquake hazard analyses depend strongly on how this distribution is interpreted: are seismic gaps areas of high hazard waiting to be filled by new earthquakes[2,3], or are the gaps aseismic and thus represent zones of low hazard[4,5]? Over the duration of California's instrumental catalogues (~35 yr), the best bet has been that earthquakes will happen where they have already happened[6]. A more than 2:1 majority of magnitude $M \geq 2$ California earthquakes that occurred between 2000 and 2005 were within 5 km of a previously observed (1970–1999) event (Fig. 1).

Long-term activity and quiescence on the San Andreas fault is analysed by grouping $M \geq 2$ catalogue earthquakes into volume bins along the mapped fault trace. Bins were 1 km × 1 km in map view, and 5 km deep. Along-fault spatial earthquake density variation is shown in Fig. 2a, where earthquake clusters and gaps are readily apparent. A spectral analysis was carried out on the trace shown in Fig. 2a using the multitaper method[7–9] to quantify significant spatial scales of earthquake activity variation.

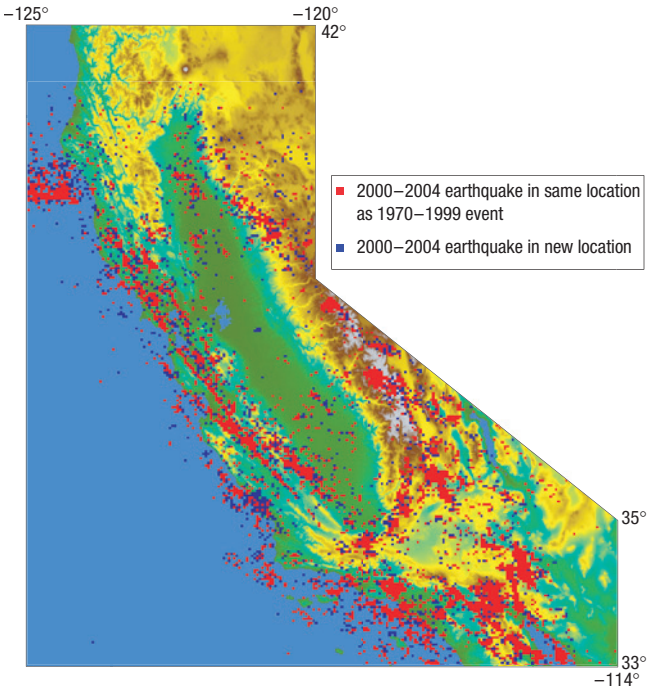

Figure 1 California seismicity. Red dots represent earthquakes that happened between 2000 and 2004 within 5 km of a previous (1970–1999) earthquake. Blue dots represent 'new' earthquake locations. Earthquakes were more likely to happen where previous events occurred by a more than 2:1 margin.

Amplitude-spectrum results show large-amplitude earthquake clustering along the San Andreas fault at inter-cluster distance scales of tens of kilometres (Fig. 2b). Significant (>95% confidence) clustering is also seen at finer scales (between 1 and 5 km), suggesting varying spatial distribution of earthquakes within larger clusters. The array of significant spectral peaks of increasing amplitude and spacing in Fig. 2b is suggestive of power-law self-similarity.

The amplitude spectrum of San Andreas fault earthquake distribution shows approximately homogeneous power-law behaviour with an exponent of −1 ($f(x) = cx^{-1}$), such that taking logarithms yields

$$\log(E_d) = c - \log(f_s), \quad (1)$$

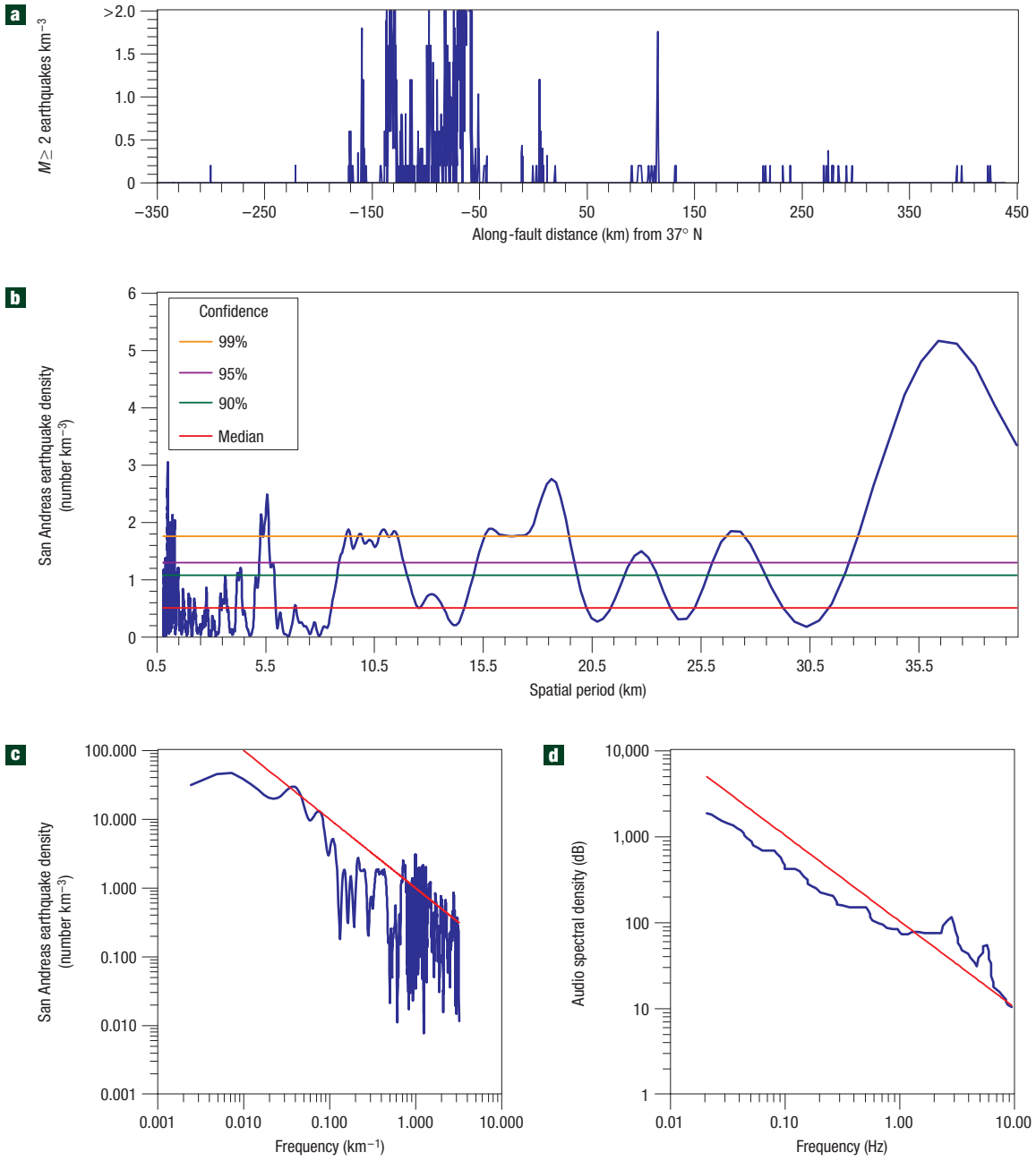

Figure 2 Amplitude spectra of San Andreas fault seismicity. a, Earthquake density (events km^{-3}) binned along the San Andreas fault shows clusters and gaps. **b**, Amplitude spectrum of the trace shown in **a**. Confidence intervals of spectral peaks are indicated. **c**, A log–log plot of earthquake density versus frequency demonstrates homogenous power-law behaviour, implying self-similarity in clusters across spatial ranges from 1 to 100 km. **d**, Homogeneous power-law behaviour occurs in well-organized structures like the array of notes used in Bach's first Brandenburg concerto[10].

where E_d is earthquake density and f_s is spatial frequency. A log–log plot of the San Andreas fault earthquake density spectrum approximates a linear relationship and is comparable to an f_s^{-1} line (Fig. 2c). The spatial pattern of San Andreas earthquakes thus shares power-law self-affinity with highly organized structures like the distribution of notes within Bach's Brandenburg concertos[10] (Fig. 2d), natural phenomena like tree and river branching[11] and fault-zone structures[12].

Earthquakes are generated by slip on faults. Fault zones like the San Andreas are noted for showing complexity like bends, steps and jogs that show self-similarity on map scales[13–15], and on individual fault surfaces[16]. Patterns of spatial earthquake distribution have been suggested as possible consequences of slip irregularity[17,18]; advances in computer power and finite-element techniques[19] have enabled a test of the link between complex structure and the distribution of earthquakes.

The question addressed here is whether observed self-affine spatial clustering of San Andreas fault earthquakes results from a heterogeneous stress distribution, and if so how long it is expected to persist. Testing was conducted using finite-element methods

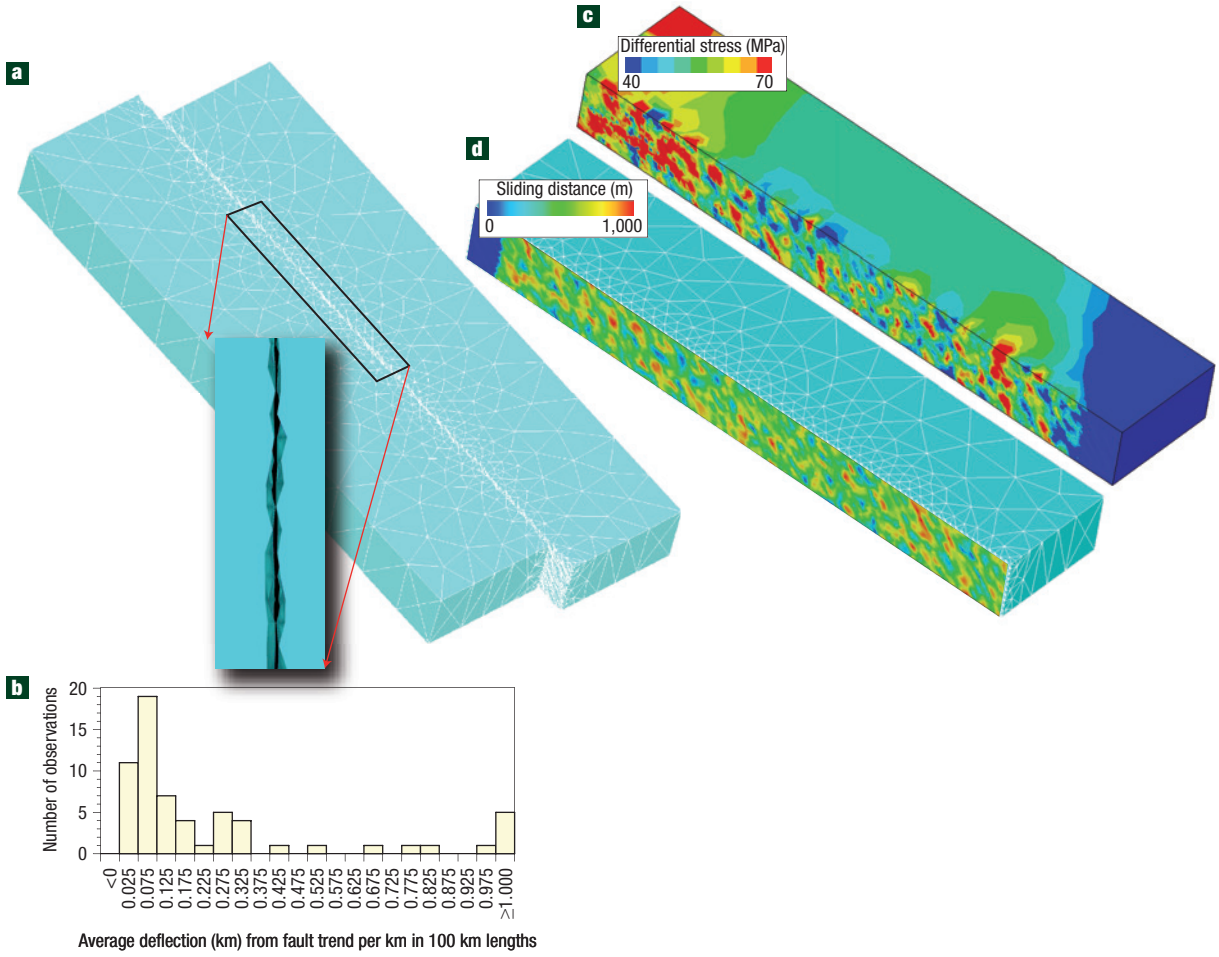

Figure 3 Finite-element model of a rough fault surface. a, Two 100-km-long blocks are surfaced with a simulated irregular fault. **b**, Observed variability in strike along the mapped trace of the San Andreas fault, from which roughness was generated. The rough fault surfaces had varying scales of contact points that, when sliding occurred during model runs, led to **c**, which shows the spatially heterogeneous distribution of differential stress. **d**, A 25,000 yr simulation at a 40 mm yr^{-1} slip rate enabled some contact points to slide by up to 1 km, which was the input wavelength of fault roughness.

that enabled accurate assessment of deformation and stress from interactions between solids with highly complex three-dimensional geometries. Models consisted of two right-laterally translating blocks sliding in contact over a simulated fault surface.

Mapped San Andreas fault traces[20] were sampled at 1 km intervals over 800 km of its length to establish fault complexity. At this scale it is appropriate to study 100 km fault lengths given that a generalized power spectrum for self-similar fault surfaces was determined to be $H \approx 0.01L$, where H is roughness and L is length[21,22]. A 100-km-long simulated fault surface was generated by randomly sampling from the distribution of observations at 1 km intervals (Fig. 3b) both along strike and to 10 km depth. Thus no assumption was made that the surface trace represents structure at depth; however, it was assumed that the 1 km scale of deflections relative to a 100 km segment length was constant to depth[21,22].

Each fault face in the finite-element model had a unique randomly generated irregular surface, which led to a heterogeneous set of contact points differing in scale and relative pressure. Further, as the model blocks slid past each other, the nature of fault contacts could change. Fault surfaces were covered with zero-thickness contact elements that had Coulomb slip criteria $CF \equiv \bar{\tau}_f + \mu(\sigma_n)$, where $\bar{\tau}_f$ is shear stress at points on contact surfaces, σ_n is normal stress or pressure directed orthogonal to surface points and μ is the friction coefficient. A Coulomb surface can show sticking and sliding behaviour. A low friction coefficient ($\mu = 0.2$) was assigned, as determined for the San Andreas fault[23–26].

Solid model blocks underlying contact elements (Fig. 3) were meshed into elements with material properties of granite[27,28]. Solid model elements had special properties intended for replicating rock behaviour. If stress concentrations exceeded strength criteria as determined from laboratory studies[27,29], elements could respond by cracking or crushing. Orientations of fracture planes were determined by magnitudes and directions of principal stress axes and the coefficient of internal friction for granite[28] ($\mu = 0.6$). Element fracturing was an essential stress-release mechanism that prevented unrealistic stress concentrations from developing on and around the rough fault surfaces. Models without rock-simulating elements produced the same results, but could not be run over as long model times.

The model blocks were translated past each other in a right-lateral sense at cumulative 40 mm yr^{-1} rates for a simulation of 25,000 yr duration. A purely elastic model would be rate independent. However, because elements could develop interacting fractures to relieve stress concentrations, their sequence of formation could be important. Therefore, the model was allowed to evolve over time steps.

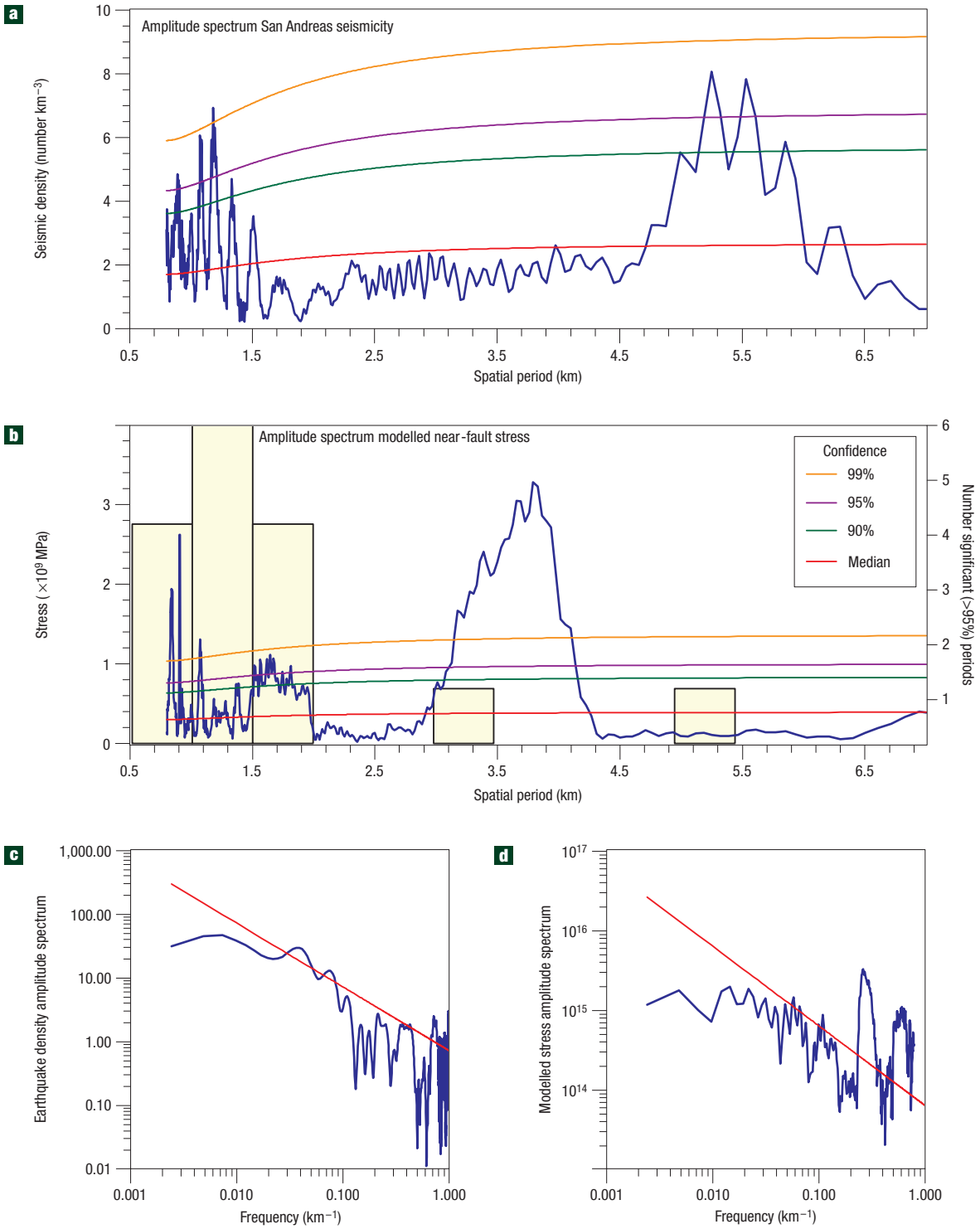

Figure 4 Amplitude spectra of modelled differential stress distribution with observed San Andreas fault seismicity. a, An example plot of spectral peaks from a 100-km-long section of the San Andreas fault for comparison with **b**, which shows calculated stress from the 100-km-long model in Fig. 3. The histogram shows the distribution of significant (95% confidence) spectral peaks of observed seismic density from eight 100 km San Andreas segments. (The legend in **b** also corresponds to **a**.) **c**, Log of seismic density is plotted against spatial frequency for comparison with **d**, where log of stress is plotted. Both relationships show homogeneous power-law behaviour between frequencies corresponding to 1–10 km cluster spacings. The implication is that slip on a modelled rough fault with parameters taken from the mapped trace of the San Andreas fault can produce a temporally stable, heterogeneous distribution of differential stress that matches characteristics of spatial earthquake distribution.

Finite-element analysis permitted tracking of simulated fault-zone processes as the model blocks moved past each other, including: (1) Coulomb stress accumulation on fault surfaces; (2) full stress and strain tensors in the underlying solids; (3) quasi-plastic deformation through element fracture; and (4) frictional heat generation. A heterogeneous distribution of

accumulated slip and differential stress (difference between greatest and least principal stresses) was quickly established in the model (Fig. 3). The spatial distribution of differential stress remained constant in time until the fault was able to evolve slip past the input 1 km irregularity scale (25,000 yr).

Modelling showed that slip on a rough, self-similar fault surface will produce a long-lived, heterogeneous distribution of differential stress that persists at least as long as it takes for displacement to equal or exceed a given spatial period of roughness. Therefore, it is expected that the broader differential stress distribution patterns would persist longer than finer-scale ones. Because differential stress ultimately drives earthquakes, the inference is that seismic clustering results from distribution of high- and low-stress regions, and that intervening gaps have few earthquakes because there is less driving stress. Slip on complex faults can then generate spatial seismic gaps that do not require filling by intermediate-magnitude earthquakes ($M \sim 6$–7) on typical earthquake-recurrence timescales (10^1 to 10^3 yr on the San Andreas fault, depending on magnitude[30]). The model did not allow significant fault generation and abandonment, which if allowed would decrease the temporal stability of modelled stress patterns.

The spectral character of modelled differential stress distribution from a 100-km-long rough fault is compared with 100 km lengths of observed San Andreas fault earthquake distribution in Fig. 4. Most of the observed significant spatial periods (inverse of frequency of seismic density variations) were found to be between 1 and 5 km (Fig. 4b), which was matched by the spectrum of modelled stress variations. Modelled stress amplitude versus frequency showed homogeneous power-law behaviour over the ~ 0.03–$1\,\mathrm{km}^{-1}$ spatial-frequency range (Fig. 4d), which corresponds to spatial periods of 1 to 30 km. The distribution takes the same form as equation (1), where $\log(\tau) = a - b \cdot \log(f_\tau)$, with τ being differential stress and f_τ spatial frequency. The slope of the stress-model power-law distribution was $b = 1.4 \pm 0.6$ (see Supplementary Information, Fig. S1), and the earthquake-density distribution had a slope of $b = 2.1 \pm 0.7$ from equation (1). Thus a model drawing randomly from observed San Andreas fault variation produces a stress distribution of the same functional form as the earthquake distribution, with similar power-law slopes. The elastic model with its single straight fault is limited in scope. If an inelastic model with multiple interacting and bending faults were introduced, it is expected that a richer spectrum of observations will be captured.

A consequence of slip on an irregular fault surface is the production of a heterogeneous stress field and accompanying heterogeneous spatial earthquake distribution. At its highest measured slip rates ($\sim$35–40 mm yr^{-1}), it would require many thousands of years for the San Andreas fault to change its pattern of fault jogs and steps. Thus the current spatial pattern of earthquake activity is likely to remain stable over the duration of hazard calculations (usually 1–50 yr). This means the most likely sites for future $M < 7$ earthquakes are sites of past events. Further, seismic gaps are likely to remain quiet because of relatively low differential stress. However, instrumental catalogue earthquakes ($M < 7.0$) used to calculate seismic-density variability did not include the largest possible San Andreas earthquakes. For example, the $M \approx 8$ 1906 and 1857 earthquakes each ruptured almost half the San Andreas fault. Dynamic stresses developed by $M \geq 7$ earthquakes may thus enable them to rupture though low-stress zones. Therefore, lower-stress gaps are not immune from earthquake slip, but are less likely nucleation sites.

Received 19 July 2007; accepted 24 October 2007; published 9 December 2007.

References

1. Kagan, Y. Y. & Knopoff, L. Spatial distribution of earthquakes: The two-point correlation function. *Geophys. J. R. Astron. Soc.* **62**, 303–320 (1980).
2. McCann, W. R., Nishenko, S. P., Sykes, L. R. & Krause, J. Seismic gaps and plate tectonics: Seismic potential for major boundaries. *Pure Appl. Geophys.* **117**, 1082–1147 (1979).
3. Nishenko, S. P. Circum-Pacific seismic potential—1989–1999. *Pure Appl. Geophys.* **135**, 169–259 (1991).
4. Kagan, Y. Y. & Jackson, D. D. Seismic gap hypothesis: Ten years after. *J. Geophys. Res.* **96**, 21419–21429 (1991).
5. Rong, Y., Jackson, D. D. & Kagan, Y. Y. Sesimic gaps and earthquakes, *J. Geophys. Res.* **108** (2003) (doi:10.1029/2002JB002334).
6. Kafka, A. L. & Ebel, J. E. Exaggerated claims about earthquake predictions. *EOS* **88**, 1–6 (2007).
7. Thomson, D. J. Spectrum estimation and harmonic analysis. *Proc. IEEE* **70**, 1055–1096 (1982).
8. Percival, D. B. & Walden, A. T. *Spectral Analysis for Physical Applications* (Cambridge Univ. Press, Cambridge, 1993).
9. Ghil, M. *et al.* Advanced spectral methods for climatic time series. *Rev. Geophys.* **40**, 3.1–3.41 (2002).
10. Voss, R. F. & Clarke, J. "1/f noise" in music: Music from 1/f noise. *J. Acoust. Soc. Am.* **63**, 258–263 (1978).
11. Schroeder, M. *Fractals, Chaos, Power Laws* (W. H. Freeman and Company, New York, 1991).
12. Scholz, C. H. *The Mechanics of Earthquakes and Faulting* (Cambridge Univ. Press, Cambridge, 2002).
13. Segall, P. & Pollard, D. D. Mechanics of discontinuous faults. *J. Geophys. Res.* **85**, 4337–4350 (1980).
14. Aviles, C. A., Scholz, C. H. & Boatwright, J. Fractal analysis applied to characteristic segments of the San Andreas fault. *J. Geophys. Res.* **92**, 331–344 (1987).
15. Okubo, P. G. & Aki, K. Fractal geometry in the San Andreas fault system. *J. Geophys. Res.* **92**, 345–355 (1987).
16. Power, W. L., Tullis, T. E., Brown, S., Boitnott, G. N. & Scholz, C. H. Roughness of natural fault surfaces. *Geophys. Res. Lett.* **14**, 29–32 (1987).
17. Kagan, Y. Y. Fractal dimension of brittle fracture. *J. Nonlinear Sci.* **1**, 1–16 (1991).
18. Marsan, D. Can coseismic stress variability suppress seismicity shadows? Insights from a rate-and-state friction model. *J. Geophys. Res.* **111** (2006) (doi:10.1029/2005JB004060).
19. ANSYS Inc, *Multiphysics Finite Element Software, Version 11* (Canonsburg, PA, 2007).
20. Jennings, C. W. Fault activity map of California and adjacent areas with locations and ages of recent volcanic eruptions. California Division of Mines and Geology Data Map Series No. 6, 92 p., 2 plates, map scale 1:750,000 (1994).
21. Brown, S. R. & Scholz, C. H. Broad bandwidth study of the topography of natural rock surfaces. *J. Geophys. Res.* **90**, 2575–2582 (1985).
22. Sagy, A., Brodsky, E. E. & Axen, G. J. Evolution of fault-surface roughness with slip. *Geology* **35**, 283–286 (2007).
23. Brune, J. N., Henyey, T. & Roy, R. F. Heat flow, stress, and the rate of slip along the San Andreas fault, California. *J. Geophys. Res.* **74**, 3821–3827 (1969).
24. Zoback, M. D. *et al.* New evidence of the state of stress of the San Andreas fault system. *Science* **238**, 1105–1111 (1987).
25. Reasenberg, P. A. & Simpson, R. W. Response of regional seismicity to the static stress change produced by the Loma Prieta earthquake. *Science* **255**, 1687–1690 (1992).
26. Geist, E. L. & Andrews, D. J. Slip rates on San Francisco Bay area faults from anelastic deformation of the continental lithosphere. *J. Geophys. Res.* **105**, 25543–25552 (2000).
27. Christensen, N. I. Poisson's ratio and crustal seismology. *J. Geophys. Res.* **101**, 3139–3156 (1996).
28. Byerlee, J. D. Friction of rocks. *Pure Appl. Geophys.* **116**, 615–626 (1978).
29. Birch, F. Compressibility; elastic constants. *Geol. Soc. Am. Mem.* **97**, 97–173 (1966).
30. Weldon, R., Scharer, K., Fumal, T. & Biasi, G. Wrightwood and the earthquake cycle: What the long recurrence record tells us about how faults work. *GSA Today* **14**, 4–10 (2004).

Acknowledgements

This work was inspired by a presentation on irregular faults by Jim Dieterich, research by David Marsan and a conversation with Larry Hartge.
Supplementary Information accompanies this paper on www.nature.com/naturegeoscience.